

# Isogeometric topology optimization of auxetic materials based on moving morphable components method

Xiaoya Zhai<sup>1,2,a</sup>, Yundong Gai<sup>3,4,b,\*</sup>, Liuchao Jin<sup>2</sup>, Wei-Hsin Liao<sup>2,\*</sup>,  
Falai Chen<sup>1</sup>, Ping Hu<sup>4</sup>

<sup>1</sup> School of Mathematical Sciences, University of Science and Technology of China, Hefei, Anhui, China

<sup>2</sup> Department of Mechanical and Automation Engineering, The Chinese University of Hong Kong, Hong Kong, China

<sup>3</sup> Hithink Royal Flush Information Network Co., Ltd., Hangzhou, Zhejiang, China

<sup>4</sup> State Key Laboratory of Structural Analysis for Industrial Equipment, School of Automotive Engineering, Dalian University of Technology, Dalian, Liaoning, China

<sup>a</sup>xiaoya\_zhai@outlook.com, <sup>b</sup>yd\_gai@foxmail.com

**Keywords:** Auxetic Materials Design, Isogeometric Topology Optimization, Microstructures Design, Moving Morphable Method, Homogenization Theory

**Abstract.** Auxetic materials are a class of materials that exhibit a negative Poisson's ratio. They have held a major interest in academics and engineering focusing on finding the material distribution and examining the mechanisms, properties, and applications. Inverse homogenization theory is taken as an effective material design tool and has been applied to optimize various metamaterials. In this paper, we derive and implement the energy-based isogeometric homogenization to generate auxetic materials. Numerical examples show that the homogenized elasticity matrix obtained by the energy-based isogeometric homogenization method is almost the same as that obtained by the finite element homogenization method within a tolerated error. On this basis, we applied the isogeometric Moving Morphable Components (MMC) method to the optimization design of auxetic materials which is named the TOP-IGA-MMC method. We further make a comparison of the Solid Isotropic Material with the Penalization (SIMP) method and the TOP-IGA-MMC method in the geometries and properties of the final optimal auxetic materials. Parameter tests and physical tests are also introduced to verify the robustness and effectiveness of the proposed method.

## Introduction

Metamaterials are engineered materials with properties usually not seen in nature such as negative Poisson's ratio (also named auxetic material) [1]. In recent years, metamaterials such as left-handed materials [2] and invisibility cloak [3] have been increasingly prominent in the fields of optics, communications, national defense, and other applications.

Generally, metamaterials are artificially optimized to achieve extraordinary properties based on topology optimization. The groundbreaking work by Sigmund [4] is assumed that microstructures are arranged periodically throughout the space, while their length scale is much smaller than those of macroscopic space. After that, topology optimization has been rapidly developed, and researchers have proposed a variety of different topology optimization methods such as Solid Isotropic Material with Penalization (SIMP) method [5], Evolutionary Structural Optimization (ESO) method [6], Level Set Method (LSM) [7], etc. However, for these existing methods, the topology optimization methods are implemented in an implicit way. The topologies only have implicit descriptions which means that the final optimized structure is detected either from a higher dimensional level set function (LSM) or a black-white binary field (SIMP and ESO

methods). In addition, for the density-based method, sensitivity analyses are carried out on a fixed finite element grid. The accuracy of analysis results highly depends on the resolution of the finite element meshes.

In order to obtain explicit boundary representations, Guo et al. [8] established an explicit topology optimization method based on the moving morphable components (MMC) method. The method takes the geometric parameters related to components as design variables. By optimizing these geometric parameters, the components can be moved, stretched, and overlapped to change the topologies. Further, an open-source 188-line MATLAB code for the MMC framework was given [9]. Later, Zhang et al. [10, 11] proposed another explicit topology optimization method in that they adopted closed B-splines and Boolean operations to represent the boundaries of holes. The topologies changed by evolving and merging their boundaries. This method has been gradually improved by [12–14]. For these explicit topology optimization methods, design variables of topology optimization are replaced by controlled parameters, and the number of design variables is reduced.

In the previously mentioned topology optimization methods, the traditional Finite Element Method [15] was adopted in numerical analysis. Gao et al. [16] summarized three deficiencies of FEM which are inexact representation, low continuity between neighboring finite elements, and low calculation efficiency to gain a high quality of the finite element mesh. To address these issues, IsoGeometric Analysis (IGA) is proposed by Hughes et al. [17] to perform the numerical analysis that is represented by non-uniform rational B-splines (NURBS). IGA overcomes these limitations by using the same basis functions to define both the geometry and the finite element model of the structure, resulting in a seamless connection between geometry and analysis. Additionally, the use of NURBS functions allows for the use of high-order splines, which can provide improved accuracy and convergence in the optimization process. In addition, many geometric standards in the industry regard NURBS as a powerful tool for geometric design. NURBS also plays an important role in CAD/CAE because of its good mathematical properties and efficient algorithms.

Inspiring above merits, some researchers combined IGA with topology optimization named Isogeometric Topology Optimization (ITO) which is a computational method used to optimize the design of mechanical structures by combining traditional numerical optimization techniques with the use of NURBS geometry representation such as isogeometric-based SIMP method [18], isogeometric-based moving morphable components [19], ITO using trimmed spline surfaces [20] and so on. It has been applied to various fields such as structural vibration [21], shell optimization [22] and meta-materials design [23].

In this work, we propose an explicit isogeometric topology optimization approach named TOP-IGAMMC, and applied this approach to the field of material design to generate auxetic materials. We first derive the isogeometric homogenization theory and compare the numerical equivalent stiffness matrix with the results of traditional homogenization theory. The matrixes are almost the same. Then we apply the isogeometric homogenization theory to do the inverse design of auxetic materials based on MMC methods. Finally, we compare our optimized results with those generated from the isogeometric SIMP method and then do parameter tests and physical tests. The results show the effectiveness and robustness of our method.

The outline of the paper is as follows. In Section 2, the theories of the MMC method and IGA-based homogenization are presented. Thereafter, the formulations of topology optimization of auxetic material are proposed in Section 3. In Section 4, numerical examples are illustrated and compared with SIMP methods. Parameter selection is also discussed. More experiments are conducted to demonstrate the performance in TOP-IGA-MMC for auxetic materials design. Section 5 closes the paper with some concluding remarks.

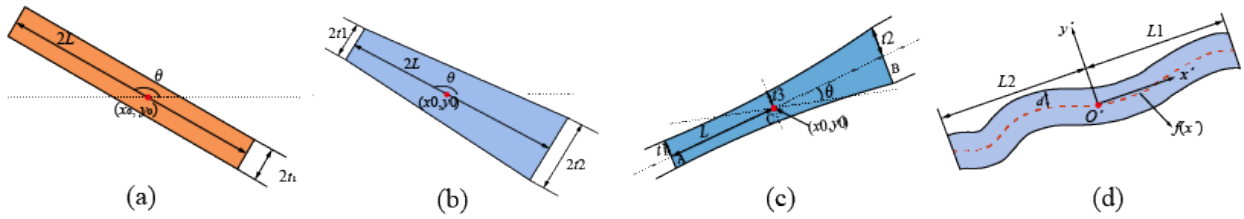


Figure 1: Geometry description of MMCs with different shapes. (a) The uniform thickness along a straight skeleton. (b) Linearly varying thickness. (c) Quadratically varying thickness. (d) The uniform thickness along the curved skeleton.

### Preliminaries

Geometry description of moving morphable components. Let  $\mathcal{D}$  represent a prescribed design domain and  $\Omega^S = \{\Omega_1, \dots, \Omega_n\}$  be a subset of  $\mathcal{D}$ .  $\Omega^S$  denotes a collection of  $n$  components. For the MMC method, there are four types of components illustrated in Paper [9] and shown in Figure 1. The components with quadratically varying thicknesses (Figure 1(c)) are chosen in this paper. For one component  $\Omega_i \in \Omega^S$ , the solid and void region is defined as follows

$$\begin{cases} \phi_i(\mathbf{x}) = 0; & \text{if } \mathbf{x} \in \partial\Omega_i; \\ \phi_i(\mathbf{x}) > 0; & \text{if } \mathbf{x} \in \Omega_i; \\ \phi_i(\mathbf{x}) < 0; & \text{otherwise;} \end{cases} \quad (1)$$

where  $\phi_i(\mathbf{x})$  ( $\forall \mathbf{x} = (x, y) \in \mathcal{D} \subset \mathbb{R}^2$ ) is an explicit topology description function, which can be defined as

$$\begin{aligned} \phi_i(\mathbf{x}) = \phi_i(x, y) &= \left(\frac{x'}{L_i}\right)^p + \left(\frac{y'}{f_i(x')}\right)^p - 1, \\ \begin{bmatrix} x' \\ y' \end{bmatrix} &= \begin{bmatrix} \cos \theta_i & \sin \theta_i \\ -\sin \theta_i & \cos \theta_i \end{bmatrix} \begin{bmatrix} x - x_{0i} \\ y - y_{0i} \end{bmatrix}, \end{aligned} \quad (2)$$

where  $(x', y')$  is the coordinate transformation of  $(x, y)$ .  $p$  is set as 6.  $(x_{0i}, y_{0i})$ ,  $L_i$  and  $\theta_i$  represent the coordinates of a center point  $O_i$ , half of the total length, and the inclination angle in the  $i$ -th component  $\Omega_i$ , respectively.  $f_i(x')$  describes the shape of the  $i$ -th component. For components with quadratically varying thickness (Figure 1(c)),  $f_i(x')$  is defined as

$$f_i(x') = \frac{t_{1i} + t_{2i} - 2t_{3i}}{2L_i^2} (x')^2 + \frac{t_{2i} - t_{1i}}{2L_i} x' + t_{3i}. \quad (3)$$

where  $t_i = \{t_{1i}, t_{2i}, t_{3i}\}$  is the thickness vector of the  $i$ -th component

These components  $\Omega^S = \{\Omega_1, \dots, \Omega_n\}$  is controlled by the parameters  $\mathbf{L} = \{L_1, \dots, L_n\}$ ,  $\mathbf{t} = \{t_{11}, t_{12}, t_{13}, \dots, t_{1n}, t_{2n}, t_{3n}\}$  and  $\boldsymbol{\theta} = \{\theta_1, \dots, \theta_n\}$ .  $n$  is the number of components. A 2D component is represented by  $\mathbf{X} = \{x_0, y_0, L, t_1, t_2, t_3, \theta\}$ . Thus, the final structure is determined by  $\mathbf{X} = \{\mathbf{X}_1^T, \dots, \mathbf{X}_n^T\}$ . When two or more components overlap, the maximum value of the topological description function  $\phi(\mathbf{x})$  ( $\forall \mathbf{x} \in \mathcal{D}$ ) of these overlapping components can be used to describe the occupied area. The final topological description function can be described as  $\phi^S = \max_i(\phi_i(\mathbf{x}))$ ,  $i = 1, \dots, n$  which is represented as

$$\begin{cases} \phi^s(\mathbf{x}) = 0; & \text{if } \mathbf{x} \in \partial\Omega^s; \\ \phi^s(\mathbf{x}) > 0; & \text{if } \mathbf{x} \in \Omega^s; \\ \phi^s(\mathbf{x}) < 0; & \text{otherwise;} \end{cases} \quad (4)$$

Isogeometric homogenization theory. The homogenization method [24, 25] is a numerical method to calculate the equivalent macroscopic properties of composites. The square domain is discretized with 4-node brick elements represented by the biquadratic NURBS elements. Given a set of points  $\mathbf{P}_{ij} \in \mathbb{R}^2$  and the corresponding weights  $w_{ij}$ , ( $i = 0, 1, \dots, m$ ,  $j = 0, 1, \dots, n$ ), a tensor product NURBS surface (the square domain) of bi-degree  $(p, q)$  is defined by

$$\mathbf{S}(\zeta, \xi) = \sum_{i=0}^m \sum_{j=0}^n R_{ij}^{pq}(\zeta, \xi) \mathbf{P}_{ij},$$

$$R_{ij}^{pq}(\zeta, \xi) = \frac{w_{ij} N_i^p(\zeta) N_j^q(\xi)}{\sum_{k=0}^m \sum_{l=0}^n w_{kl} N_k^p(\zeta) N_l^q(\xi)} \quad (5)$$

where  $\zeta \in [\zeta_p, \zeta_{m+1}]$ ,  $\xi \in [\xi_q, \xi_{n+1}]$ ,  $i = 0, 1, \dots, m$ ,  $j = 0, 1, \dots, n$  are bivariate NURBS basis functions defined over the knot vectors  $\zeta = \{\zeta_0, \zeta_1, \dots, \zeta_{m+p+1}\}$  and  $\xi = \{\xi_0, \xi_1, \dots, \xi_{n+q+1}\}$  with weights  $\{w_{ij}\}_{i=0, j=0}^{m, n}$ .  $N_i^p(\zeta)$  and  $N_j^q(\xi)$  are the B-spline basis function defined by the Cox-de Boor algorithm [26]. In addition, the macroscopic equivalent properties of the unit cell are calculated based on NURBS basis. Thus, the isogeometric homogenization theory is derived.

The homogenized equivalent elastic matrix  $\mathbf{D}_{ijkl}^H$  is obtained by averaging the integral over  $Y$  in the Einstein index, there is

$$\mathbf{D}_{ijkl}^H = \frac{1}{|Y|} \int_Y \mathbf{D}_{pqrs} \left( \epsilon_{pq}^{0(ij)} - \epsilon_{pq}^{*(ij)} \right) \left( \epsilon_{rs}^{0(kl)} - \epsilon_{rs}^{*(kl)} \right) dY, \quad (6)$$

where  $\mathbf{D}_{pqrs}$  is a locally varying elasticity tensor.  $|Y|$  is the volume of the unit cell.  $\epsilon_{rs}^{0(kl)}$  is the predefined strain field,  $\epsilon_{rs}^{*(kl)}$  is the  $Y$ -periodic solution of the following equation

$$\int_Y \mathbf{D}_{ijrs} \epsilon_{ij}(v) \epsilon_{rs}^{*(kl)} dY = \int_Y \mathbf{D}_{ijrs} \epsilon_{ij}(v) \epsilon_{rs}^{0(kl)} dY, \quad (7)$$

where  $v$  is a virtual displacement field.  $\epsilon_{rs}^{(kl)} = \epsilon_{rs}^{0(kl)} = \epsilon_{rs}^{*(kl)}$  is superimposed strain field. In the isogeometric homogenization, one unit cell is modeled by NURBS representation with open node vectors and can be rewritten as the discrete form

$$\mathbf{D}_{ijkl}^H = \frac{1}{|Y|} \sum_{e=1}^{N_e} d_e^{(ij)} \mathbf{K}_e d_e^{(kl)} \quad (8)$$

where  $\mathbf{K}_e = \rho_e^p \mathbf{K}_e^0$ ,  $\rho_e$  is the density of the NURBS element.  $p$  is the penalty parameters,  $\mathbf{K}_e^0$  is the solid stiffness matrix.  $N_e$  is the number of elements.  $d_e^{(ij)}$  is the displacement field defined on the NURBS elements. We modified the Eq. (8) by replacing engineering notation instead of Einstein notation using  $11 \rightarrow 1$ ,  $22 \rightarrow 2$ ,  $12 \rightarrow 3$ . So Eq. (8) is rewritten as

$$\mathbf{D}_{ij}^H = \frac{1}{|Y|} \sum_{e=1}^{N_e} d_e^{(i)} \mathbf{K}_e d_e^{(j)} \quad (9)$$

Under the periodic assumption, the displacement field  $d_i$  of one unit cell can be expressed as the sum of the macroscopic displacement field  $\epsilon_{ij}^0 y_j$  and the microscopic periodic perturbation displacement  $d^*$ , that is

$$d_i = \epsilon_{ij}^0 y_j + d^* \tag{10}$$

where  $d_1$  and  $d_2$  represent the displacement along  $x$  and  $y$  directions. For a 2D unit cell, the displacement of the pairs of opposite sides is respectively

$$\begin{cases} d_i^{k+} = \epsilon_{ij}^0 y_j^{k+} + d^* \\ d_i^{k-} = \epsilon_{ij}^0 y_j^{k-} + d^* \end{cases} \tag{11}$$

where the superscripts  $k +$  and  $k -$  represent the top (right) and bottom (left) lines perpendicular to the  $k$ -th direction ( $k = 1$  ( $x$  direction) or  $2$  ( $y$  direction)), respectively. Since the periodic perturbation displacement field  $d^*$  is unknown,  $d^*$  can be eliminated by calculating the displacement difference between the opposite side  $k +$  and  $k -$ , then

$$w_i^k = d_i^{k+} - d_i^{k-} = \epsilon_{ij}^0 (y_j^{k+} - y_j^{k-}) = \epsilon_{ij}^0 \Delta y_j^k \tag{12}$$

For the NURBS patch, the first and last control points in the  $k$ -th direction are interpolated on the cell boundary, thus  $\Delta y_1^1 = y_1^0$ ,  $\Delta y_1^2 = 0$ ,  $\Delta y_2^1 = 0$ , and  $\Delta y_2^2 = y_2^0$ . In the horizontal direction, the displacement difference between the left and right sides of a unit cell is  $w_1^1 = \epsilon_{1j}^0 y_1^0$ ; Vertically, the difference between the top and bottom of the cell is  $w_2^2 = \epsilon_{2j}^0 y_2^0$ .

### Methods

The TOP-IGA-MMC method is applied to the topology optimization for auxetic materials design. The proposed model is given in subsection 3.1. Then the detailed sensitivity analysis is introduced. Finally, the optimization process is summarized in algorithm 1.

---

**Algorithm 1:** The TOP-IGA-MMC method

---

**input :** Numbers of elements along  $x$  and  $y$  direction are  $nelx$  and  $nely$ ; the upper limit of the volume fraction is set as  $V^*$  and the penalty factor  $p$ ;  
**output:** Optimized components.  
 1 Initialization: The parameters of initial components  $X_k = \{x_{0k}, y_{0k}, L_k, t_{1k}, t_{2k}, t_{3k}, \theta_k\}$   $\forall k$ ; the iteration index  $i = 0$ ; design change  $\Delta = 1.0$ ; threshold  $\epsilon = 10^{-3}$ ;  
 2 **while**  $\Delta > \epsilon$  &  $i < I_{max}$  or  $i \leq I_{min}$  **do**  
 3      $i = i + 1$ ;  
 4     Calculate the equilibrium equation via. Eq. (16).  
 5     Compute objective function and volume constraints via Model (13);  
 6     Evaluate  $\frac{\partial J}{\partial X}$  via Eq.(18);  
 7     Update  $X^{[i]}$  via MMA solver;  
 8      $\Delta = \max_{\forall k} (|X_k^{[i]} - X_k^{[i-1]}|)$ ;  
 9 **end**

---

Model formulation. In TOP-IGA-MMC, MMCs are used as the basic units to describe the structural topologies. The component with quadratically varying thickness is adopted. The geometric description parameters  $\mathbf{X} = \{\mathbf{X}_1^T, \dots, \mathbf{X}_n^T\}$  are taken as the design variables. The model is formulated by optimizing the negative Poisson's ratio under the predefined volume  $V^*$ . The objective function follows the relaxation form in Paper [27]. Therefore, the optimization model of topology optimization for auxetic materials can be written as

$$\begin{aligned}
 &\text{find:} && \mathbf{X} = \{\mathbf{X}_1^T, \dots, \mathbf{X}_n^T\} \\
 &\min_{\mathbf{X}} && J(\mathbf{D}^H(\boldsymbol{\rho})) = D_{12}^H - \gamma^l(D_{11}^H + D_{22}^H) \\
 &\text{s. t.} && \mathbf{Kd} = \mathbf{F} \\
 &&& \sum_e \frac{\rho_e v_e}{|Y|} \leq V^* \\
 &&& 0 \leq \rho_e \leq 1
 \end{aligned} \tag{13}$$

where  $X_i = \{x_{0i}, y_{0i}, L_i, t_{1i}, t_{2i}, t_{3i}, \theta_i\}$  ( $i = 1, \dots, n$ ) is the geometric parameters. In the objective function  $J$ ,  $l$  is the number of iteration steps and  $\gamma = 0.8$ .  $\mathbf{D}^H(\boldsymbol{\rho})$  is the homogenized equivalent elastic matrix based on engineering notation calculated by Eq. (9). The element density  $\rho_e$  is represented as

$$\rho_e = \sum_{j=1}^{N_g} \kappa_j \left( \sum_{i=1}^{N_{cp}} R_i(\zeta_j, \xi_j) H(\phi_{i,e}) \right) \tag{14}$$

where  $N_g$  is the number of Gauss points in one element.  $\kappa_j$  is the coefficients of the Gaussian integral.  $\phi_{i,e}$  ( $i = 1, \dots, N_{cp}$ ) is value of topological description function  $\phi_s(x)$  at the  $i$ -th control point of the  $e$ -th element.  $N_{cp}$  is the number of control points.  $R_i(\zeta_j, \xi_j)$  is non-uniform rational B-splines basis in Eq. (5). The Heaviside function  $H(x)$  is

$$H_\epsilon(x) = \begin{cases} 1, & \text{if } x > \epsilon \\ \frac{1(1-\alpha)}{4} \left( \frac{x}{\epsilon} - \frac{x^3}{3\epsilon^3} \right) + \frac{1+\alpha}{2}, & \text{if } -\epsilon < x \leq \epsilon \\ \alpha, & \text{otherwise} \end{cases} \tag{15}$$

where  $\alpha$  is a constant value that is very small to avoid the singularity of the stiffness matrix.  $\epsilon$  is used to describe the function regularization.  $v_e$  is volume of the  $e$ -th element.  $|Y|$  is the volume of the single cell.  $V^*$  is the upper limit of the volume fraction. Young's modulus is represented as  $E_e(\rho_e) = E_{min} + \rho_e^p (E_0 - E_{min})$ .  $E_0$  and  $E_{min} = 10^{-9}$  are Young's modulus of solid and void materials.  $p$  is the penalty factor.  $\mathbf{Kd} = \mathbf{F}$  is equilibrium equation. The displacement  $\mathbf{d}$  of all control points is divided into four parts. Among them,  $\bar{\mathbf{d}}_1$  represents the known displacement of the four corner control points;  $\mathbf{d}_3$  and  $\mathbf{d}_4$  represent the displacement of other control points on the boundary of one unit cell, which should satisfy  $\mathbf{d}_4 = \mathbf{d}_3 + \bar{\mathbf{w}}$ ;  $\bar{\mathbf{w}}$  can be obtained from Eq. (12);  $\mathbf{d}_2$  represents the unknown displacement of all internal control points. Then the equilibrium equation can be written as

$$\begin{bmatrix} \mathbf{K}_{11} & \mathbf{K}_{12} & \mathbf{K}_{13} & \mathbf{K}_{14} \\ \mathbf{K}_{21} & \mathbf{K}_{22} & \mathbf{K}_{23} & \mathbf{K}_{24} \\ \mathbf{K}_{31} & \mathbf{K}_{32} & \mathbf{K}_{33} & \mathbf{K}_{34} \\ \mathbf{K}_{41} & \mathbf{K}_{42} & \mathbf{K}_{43} & \mathbf{K}_{44} \end{bmatrix} \begin{bmatrix} \bar{\mathbf{d}}_1 \\ \mathbf{d}_2 \\ \mathbf{d}_3 \\ \mathbf{d}_4 \end{bmatrix} = \begin{bmatrix} \mathbf{F}_1 \\ \mathbf{F}_2 \\ \mathbf{F}_3 \\ \mathbf{F}_4 \end{bmatrix} \tag{16}$$

where  $\mathbf{K}$  is the global stiffness matrix, and  $\mathbf{F}_1$  is the reaction force of angular control point under a given displacement.  $\mathbf{F}_2 = 0$ , and  $\mathbf{F}_3 = -\mathbf{F}_4$  under the periodic assumption. Then we have

$$\begin{bmatrix} \mathbf{K}_{22} & \mathbf{K}_{23} + \mathbf{K}_{24} \\ \mathbf{K}_{32} + \mathbf{K}_{42} & \mathbf{K}_{33} + \mathbf{K}_{34} + \mathbf{K}_{43} + \mathbf{K}_{44} \end{bmatrix} \begin{bmatrix} \mathbf{d}_2 \\ \mathbf{d}_3 \end{bmatrix} = - \begin{bmatrix} \mathbf{K}_{21} \\ \mathbf{K}_{31} + \mathbf{K}_{41} \end{bmatrix} \mathbf{d}_1 - \begin{bmatrix} \mathbf{K}_{24} \\ \mathbf{K}_{34} + \mathbf{K}_{44} \end{bmatrix} \bar{\mathbf{w}} \tag{17}$$

Solve the above linear equations, the displacement  $\mathbf{d}$  is obtained. It is worth noting that all variables are defined at the control points of NURBS elements.

Sensitivity analysis. We take  $\mathbf{b}$  as the design variables in  $\mathbf{X} = \{x_0, y_0, L, t_1, t_2, t_3, \theta\}$ , then the sensitivity of the objective function  $J(D_{ij}^H)$  to the design variable  $b$  is

$$\begin{aligned} \frac{\partial J}{\partial b} &= \sum_{i=1}^3 \sum_{j=1}^3 \frac{\partial J}{\partial D_{ij}^H} \frac{\partial D_{ij}^H}{\partial b} \\ \frac{\partial D_{ij}^H}{\partial b} &= \frac{p}{|Y|} \sum_{e=1}^{N_e} \rho_e^{p-1} \left[ \sum_{j=1}^{N_g} \frac{1}{N_g} \left( \sum_{i=1}^{N_{cp}} R_i(\zeta_j, \xi_j) \frac{\partial H(\phi_{i,e})}{\partial b} \right) \right] d_e^{(i)} \mathbf{K}_e d_e^{(j)} \end{aligned} \quad (18)$$

The sensitivity of the volume constraint function  $V$  to the design variable  $b$  is

$$\frac{\partial V}{\partial b} = \frac{v_e}{|Y|} \sum_{e=1}^{N_e} \left[ \sum_{i+g=1}^{N_g} \frac{1}{N_g} \left( \sum_{i=1}^{N_{cp}} \frac{\partial H(\phi_{i,e})}{\partial b} \right) \right] \quad (19)$$

Algorithm. The size of one unit cell is set as  $L_x \times L_y = 1 \times 1$ , the parameter  $\gamma = 0.8$  in the objective function  $J(D^H(\boldsymbol{\rho}))$  in Model (13). The convergence criterion is the maximum change  $\Delta$  of the design variables between two iterations is less than  $\epsilon$ , that is,  $\Delta \leq \epsilon$ . The Greville points are used as the control points of the elements. Young's modulus and Poisson's ratio of the solid material are set as  $E_0 = 1$  and  $\mu = 0.3$ . In order to avoid premature convergence conditions, the minimum iteration steps are set as  $I_{min} = 50$  and the maximum iteration times as  $I_{max} = 500$ . To solve the optimization problem numerically, the Method of Moving Asymptotes (MMA) [28] is used as the optimizer.

### Discussion

To verify the effectiveness of the proposed TOP-IGAMMC method for auxetic material design, we make a comparison between the TOP-IGA-MMC method and another density-based method in the numerical performances, material properties, and geometries. All the examples are run on a desktop computer: the CPU is the 11th Gen Intel(R) Core(TM) i7-1165G7 2.80GHz, the RAM is 64GB, the OS is Windows 10, and the software environment is MATLAB 2022b. The code for this paper is at <https://github.com/xiaoyazhai/TOPIGA-MMC-Micro>.

Comparisons. In order to compare the results of the proposed algorithm with those of the SIMP method, we first briefly introduce the model based on the isogeometric SIMP method named TOP-IGA-SIMP for material design. In the TOP-IGA-SIMP method, design variables are the element densities  $\rho_e$  and the objective function and constraints are the same as those in Model (13). To avoid the checkerboard patterns and obtain better structural topology, filtered sensitivity or density is often used to participate in the optimization process. For implementation details, please refer to Supplementary 5.

The optimal design of auxetic materials obtained by the TOP-IGA-MMC method and TOP-IGA-SIMP method is presented in Figure 2. The number of elements  $N$  of these two methods is set as  $50 \times 50$ . The penalty factor is 5, the volume fraction is 0.3. The number of components is 40. For all elements,  $t_1 = t_2 = t_3 = 0.05$  and  $\theta = 0$  are the initial inputs. Thus, the initial parameter combination is  $(N, p, V^*, L, t, \theta) = (50 \times 50, 5, 0.3, 0.25, 0.05, 0)$ . These two methods are compared in three aspects: numerical performances, material properties, and geometries. For the numerical performances, there are some oscillations during the first 100 iterations. Large structure changes (shown in intermediate structures of Iter=2, 8, 25, 50, 80) cause this phenomenon. The Poisson's ratio of these two optimized structures is  $-0.6124$  and  $-0.3166$ . Our method can get better results under the same number of elements. In Figure 2(b), the final result has a large number of gray densities, which will cause the instability of the results. We further increase the number of elements of the TOP-IGA-SIMP method to  $100 \times 100$  and  $200 \times 200$ , and the Poisson's ratio values of the final results are  $-0.4988$  and  $-0.6026$ , respectively. When

the number of elements is  $200 \times 200$ , the Poisson's ratio of the optimized structure is very similar to that of our method. But the time consumption is about 2.5 times that of our algorithm. In order to show more comparative results, we optimize auxetic materials under different volume fraction constraints (shown in Figure 3).

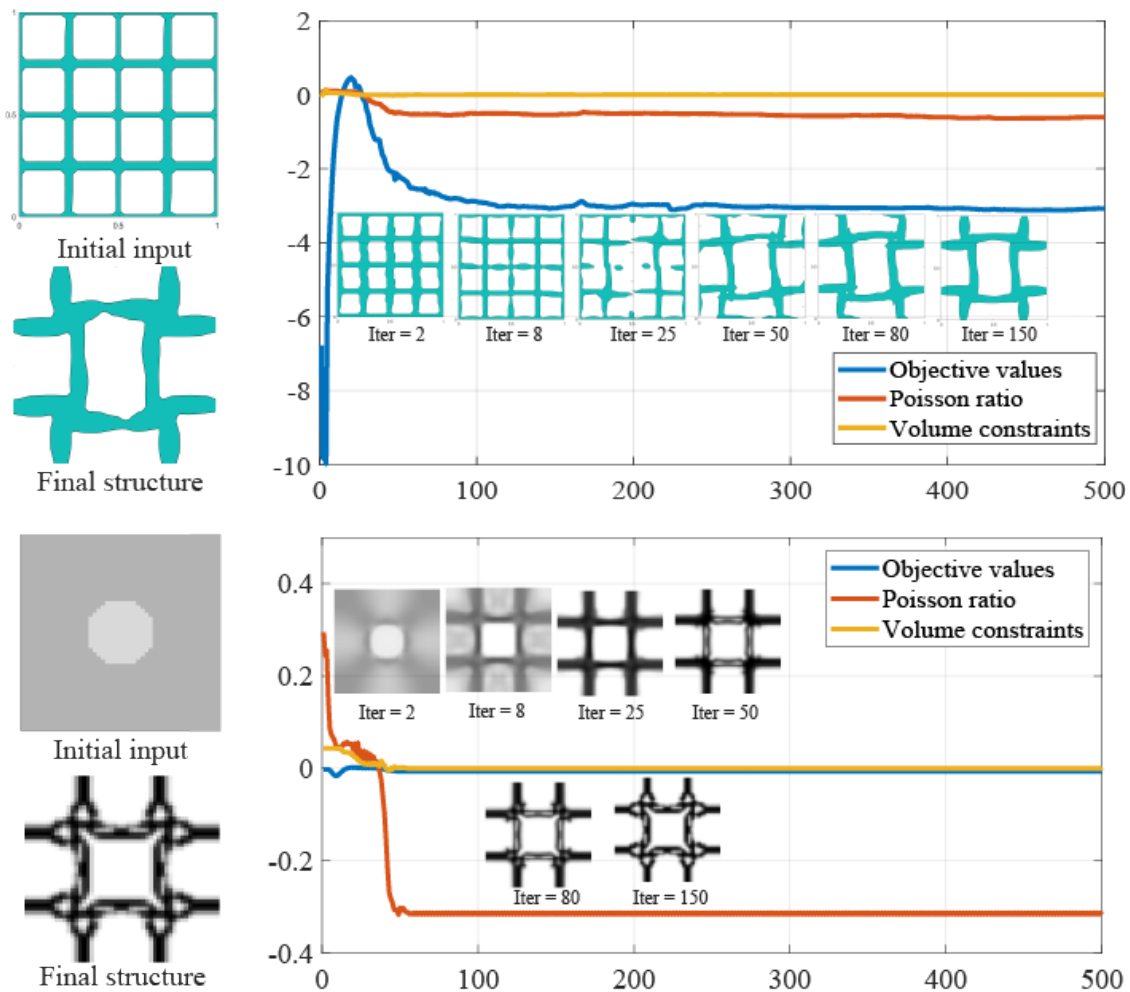


Figure 2: Plots of iteration curves of TOP-IGA-MMC method and TOP-IGA-SIMP method under the volume fraction 30%. The initial input and final optimized auxetic material are given on the left. The objective functions, Poisson's ratio, and volume constraints are plotted in the red, blue, and yellow curves. The initial parameter combination is  $(N, p, V^*, L, t, \theta) = (50 \times 50, 5, 0.3, 0.25, 0.05, 0)$ .

In Figure 3, the volume fraction constraints increase from 30% to 70%. Figure 3 (a) represents the results obtained based on the TOPIGA-MMC method. The initial parameters for the component are the same as in Figure 2. Figure 3(b)-(c) show the results under different element numbers ( $50 \times 50$  vs.  $100 \times 100$  vs.  $200 \times 200$ ) of the TOP-IGA-SIMP method. With the increase of elements numbers, the gray densities gradually decrease and there are more and more details in the final optimized structures. Whereas very small structures are not conducive to manufacturing, the result of our method is more suitable for manufacturing due to the final structures of components consolidation and clear boundaries. A discussion of the element numbers of the TOP-IGA-MMC method is covered in Section 4.2.2.



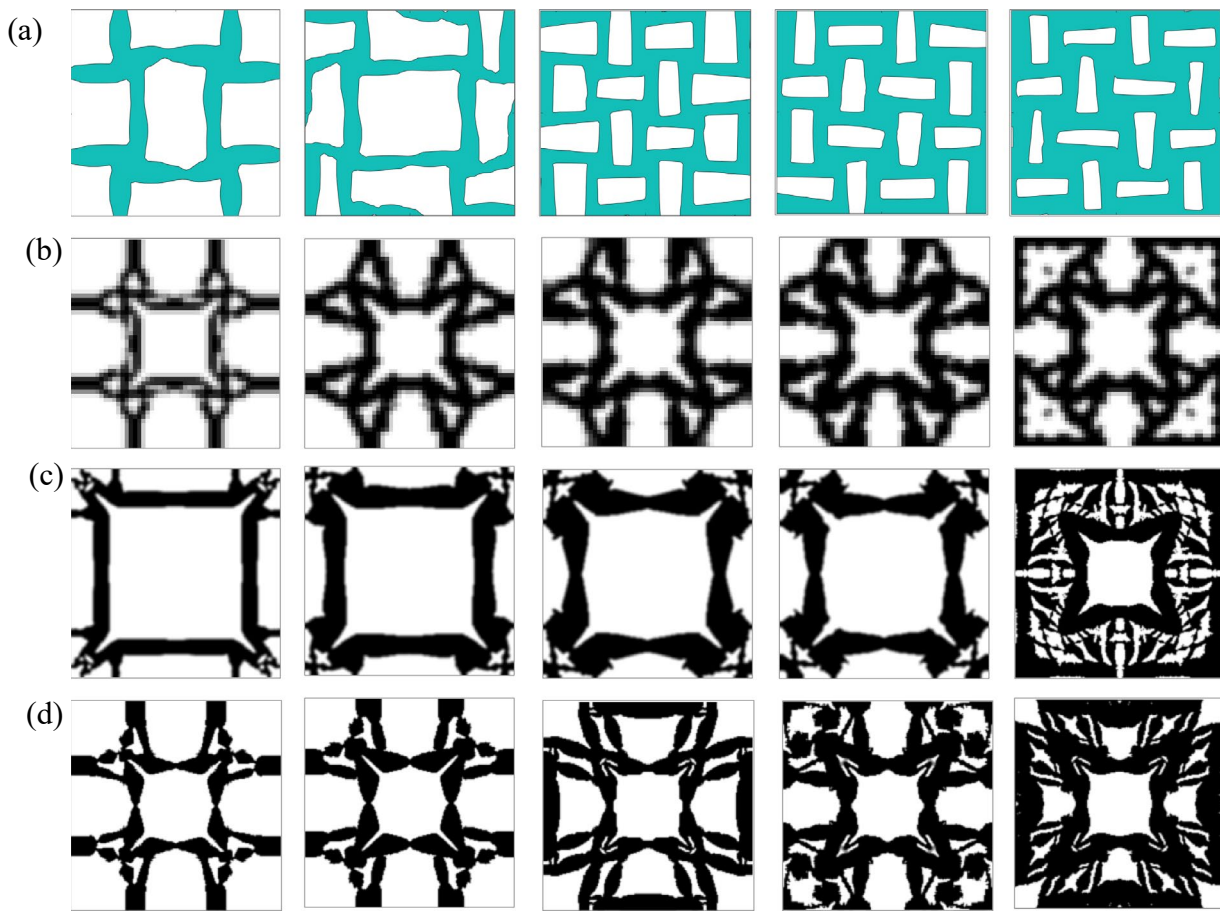




Figure 3: Different optimized auxetic materials based on TOP-IGA-MMC method (a) and TOP-IGA-SIMP method (b)-(d). The volume fraction increases gradually from left (30%) to right (70%). The number of elements is  $50 \times 50$ (a)(b),  $100 \times 100$ (c),  $200 \times 200$  (d).

Numerical tests. In this section, we first verify the calculation of the elastic matrix based on isogeometric homogenization theory by comparing with calculation methods in Paper [27] and Paper [29]. In addition, there are many local minima in the topological optimization materials design due to optimization parameters such as penalty factor  $p$ , and initialization inputs ( $L$ ,  $t$  and  $\theta$ ). Different optimization parameters and the initial components are set to analyze the impact on the generation of auxetic materials.

Numerical validation. A square cell with a central hole is taken as a calculation example. The size of the cell is  $L_x \times L_y = 1 \times 1$ , and the radius of the central hole is  $\frac{\min(\text{nel}_x, \text{nel}_y)}{3}$  and  $\frac{\min(\text{nel}_x, \text{nel}_y)}{6}$ .  $\text{nel}_x$  and  $\text{nel}_y$  are the numbers of elements along  $x$  and  $y$  directions. The initial parameter combination for TOP-IGA-MMC method is  $(N, p, V^*, L, t, \theta) = (50 \times 50, 5, 0.3, 0.25, 0.05, 0)$ . Homogenize function in [29], topX function in [27], and the proposed isogeometric homogenization method are used to calculate an equivalent elastic matrix, respectively. The comparison results are given in Table 1. It can be seen that the equivalent elastic matrices obtained by different methods are almost the same, and the maximum error is less than  $10^{-4}$ .

Table 1: The homogenized effective elasticity matrices obtained from different methods (TopX [27] vs. Homogenization [29] vs. Ours).

Initial inputs	TopX [27]	Homogenization [29]	Ours
	$\begin{bmatrix} 0.0732 & 0.0186 & 0.0000 \\ 0.0186 & 0.0732 & 0.0000 \\ 0.0000 & 0.0000 & 0.0199 \end{bmatrix}$	$\begin{bmatrix} 0.0732 & 0.0185 & 0.0000 \\ 0.0185 & 0.0732 & 0.0000 \\ 0.0000 & 0.0000 & 0.0199 \end{bmatrix}$	$\begin{bmatrix} 0.0732 & 0.0186 & -0.0000 \\ 0.0186 & 0.0732 & -0.0000 \\ -0.0000 & -0.0000 & 0.0199 \end{bmatrix}$
	$\begin{bmatrix} 0.1157 & 0.0344 & 0.0000 \\ 0.0344 & 0.1157 & 0.0000 \\ 0.0000 & 0.0000 & 0.0394 \end{bmatrix}$	$\begin{bmatrix} 0.1157 & 0.0343 & 0.0000 \\ 0.0343 & 0.1157 & -0.0000 \\ 0.0000 & -0.0000 & 0.0394 \end{bmatrix}$	$\begin{bmatrix} 0.1158 & 0.0344 & -0.0000 \\ 0.0344 & 0.1158 & -0.0000 \\ -0.0000 & -0.0000 & 0.0394 \end{bmatrix}$

Initial inputs. Number of components. The initial components and final structural topologies are shown in Figure 4. The initial parameter combination of these two cases is  $(N, p, V^*, L, t, \theta) = (40 \times 40, 3, 0.5, 0.5, 0.08, 0)$  and  $(40 \times 40, 3, 0.5, 0.25, 0.08, 0)$ . The number of components is related to the components' thickness  $L$ . In Figure 4(a), the number of components is 12, and since each component can be described with 7 parameters  $\mathbf{X} = \{x_0, y_0, L, t_1, t_2, t_3, \theta\}$ , the number of design variables is 84. In Figure 4(b), the number of components is 40 and the number of design variables is 280. The final topologies are very similar but the value of negative Poisson's ratios are  $-0.4996$  and  $-0.3307$ , respectively. Poisson's ratio is sensitive to the small difference between structures, but the different number of components has little effect on the topologies of the structures.

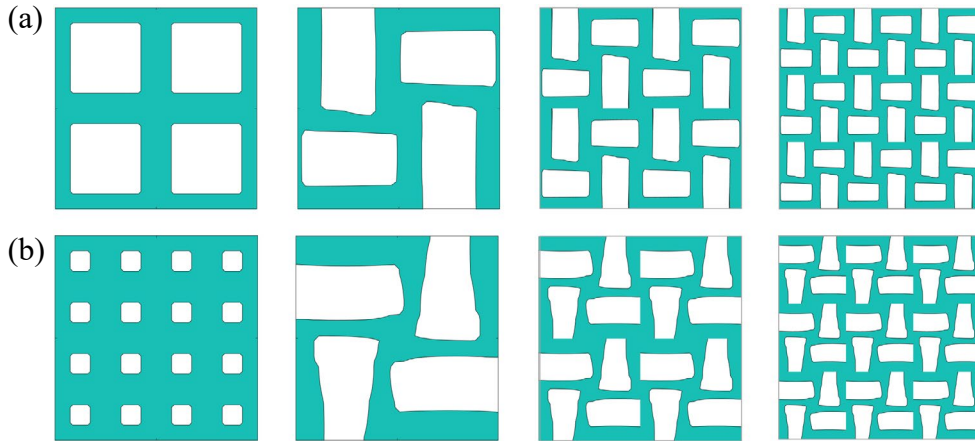
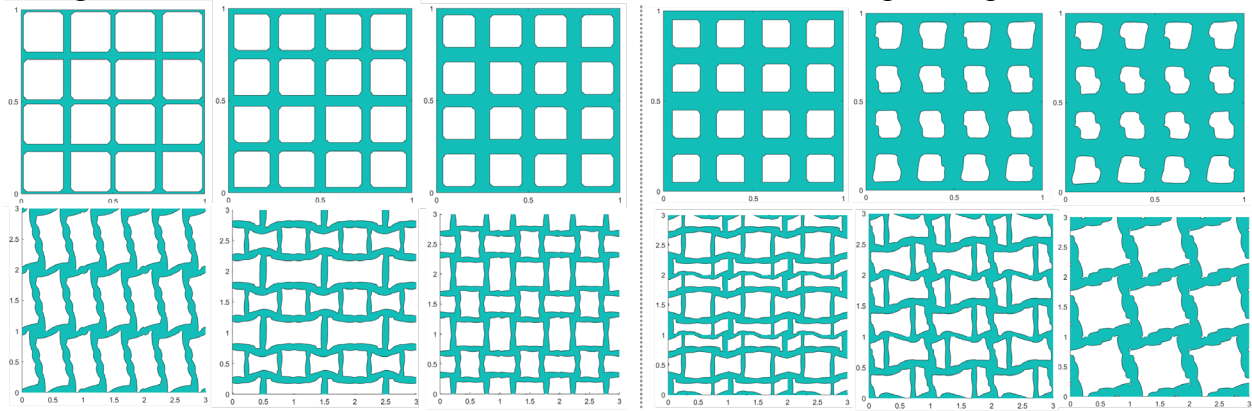


Figure 4: Comparison of a different number of components under the volume fraction 50%. (a) The number of components is 12.  $(N, p, V^*, L, t, \theta) = (40 \times 40, 3, 0.5, 0.5, 0.08, 0)$  (b) The number of components is 40.  $(N, p, V^*, L, t, \theta) = (40 \times 40, 3, 0.5, 0.25, 0.08, 0)$  The first column is initial inputs. The second column is the final topologies followed by the results of an arrangement of four and nine cells.

Geometric parameters. In addition to the number of components, the geometric parameters of the initial components also affect the optimization results, that is the components' thickness  $t_1, t_2, t_3$  and the angle  $\theta$ . We change these parameters and show the optimized results in Figure 5. Parameter testing is optimized based on  $50 \times 50$  elements. The left three columns are the test results for different thicknesses  $t$ , where the  $\theta = 0$  and the predefined volume fraction is 35%. The Poisson's ratio values are  $-0.5413, -0.3302$  and  $-0.6641$ . The right three columns are results from different angles  $\theta$ , where the component has a thickness of 0.05 ( $t_1 = t_2 = t_3$ ) and a predefined volume fraction is 40%. The penalty factor of both tests is 5. The Poisson's ratio values are  $-0.3146, -0.3157, \text{ and } -0.5115$ . The first row in Figure 5 shows the initial inputs. The structures shown in the second row of Figure 5 are the optimization results periodically arranged by  $3 \times 3$ .

Different parameter selections will affect the geometry and Poisson’s ratio of the final result. After testing, the value range of thickness is  $t \in [0, 0.1]$ , and the value range of angle is  $\theta \in [0, 0.1]$ .



(a) Different component thickness  $t$ . (b) Different component angle  $\theta$ .

Figure 5: Illustration of different geometric parameters of components.

Other parameters. The number of elements and the penalty factors are further tested and shown in Figure 6 under the same volume fraction 50%, the same initial inputs component length  $L = 0.25$ , thickness  $t_1 = t_2 = t_3 = 0.05$ , and the same initial input component angle  $\theta = 0$ . Since geometries of the TOP-IGAMMC method are controlled by the optimized components not defined on the elements, there are no grey densities in the final results. The increase in the element number helps to improve the calculation accuracy. The number of elements has little effect on the geometric results, but Poisson’s ratio values are sensitive to the small difference between different structures. In addition, we also give the optimization results of different penalty factors ( $p = 3$  and 5) in Figure 6. The final geometries are similar, but the performance is improved.

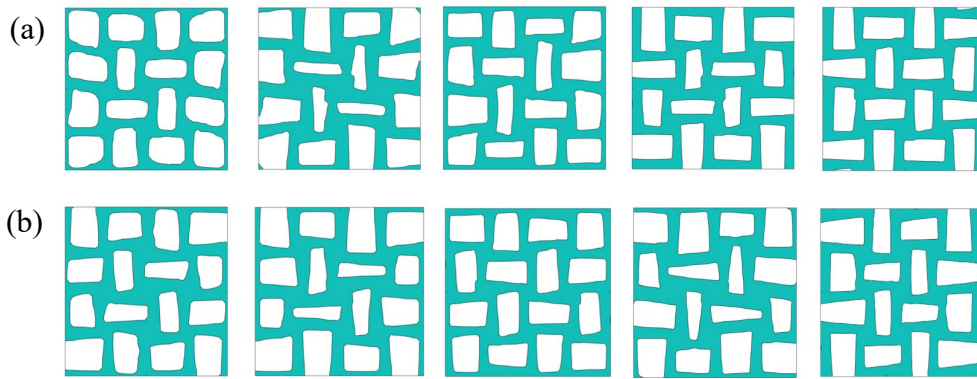


Figure 6: Different optimized auxetic materials under the volume fraction 50% by testing different element numbers and penalty factors (from left to right:  $40 \times 40$ ,  $50 \times 50$ ,  $60 \times 60$ ,  $70 \times 70$ , and  $80 \times 80$ ). (a) penalty factor  $p = 3$ ; (b) penalty factor  $p = 5$ .

Physical tests. In order to compare experimental measurements with numerical results, we print the two optimized auxetic structures by thermoplastic polyurethane (TPU). CMT5105 universal Electromechanical Testing Machine from MTS Systems Corporation in Canada is adopted to test the Poisson’s ratio. The tensile tests were conducted at predefined speeds 50 mm/min. The patterns in Figure 7(a) are the optimized structures based on the TOP-IGA-MMC method. The parameters are the same as Figure 2 and Figure 4 (b). Figure 7(b) is the experimental operating status. In addition, we also simulate the deformation and equivalent stresses of these two auxetic structures, as shown in Figure 7(c) and (d). After experimental tests and numerical simulation, the designed structures do have the property of negative Poisson’s ratio.

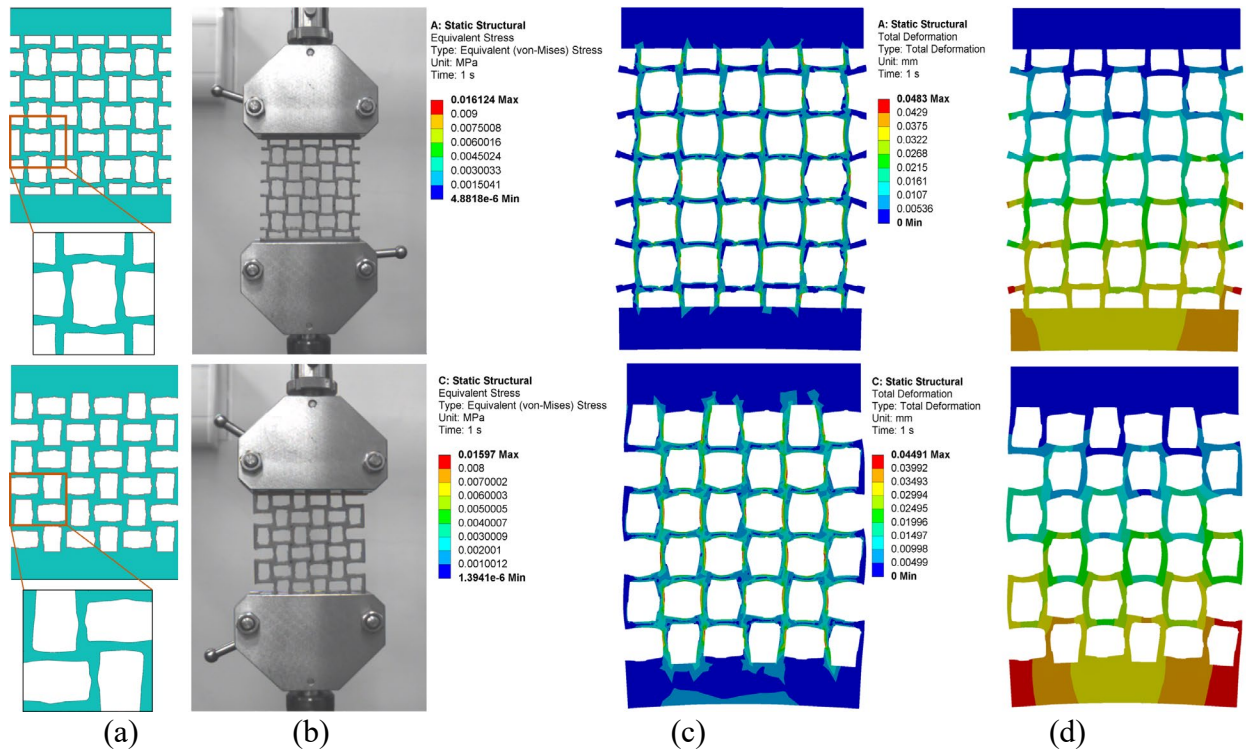


Figure 7: Physical tests and numerical simulations of two auxetic structures generated by the proposed TOP-IGA-MMC method. (a) The optimized auxetic structures and print models. (b) Physical tests. (c) Equivalent stress distribution of maximum deformation status. (d) Colormaps of total deformation distribution.

### Conclusion and Future Work

In this work, an explicit isogeometric topology optimization method, TOP-IGA-MMC, is developed. Compared with implicit topology optimization methods (such as the SIMP method), explicit topology optimization methods can avoid checkerboard patterns, gray densities, boundary diffusion, and other numerical instability phenomena. The proposed method inherits the feature that the MMC topology optimization method can express the structure topology explicitly by fewer design variables. At the same time, it has the advantages of high continuity and high calculation accuracy of isometric analysis based on higher-order NURBS basis function.

2D Auxetic materials are generated by the TOP-IGAMMC method. For an equivalent elastic matrix calculation, the isogeometric homogenization theory is illustrated. In order to verify the accuracy of the calculation, we compare it with the algorithms proposed [27, 29]. The maximum error is less than  $10^{-4}$ . Then, the TOPIGA-SIMP method is also compared with ours in numerical performances, material properties, and geometric topologies. Furthermore, the computational accuracy is improved by IGA to obtain a more accurate objective function and constraints. Hence, the proposed TOP-IGA-MMC is efficient and accurate and has great potential to solve 2D topology optimization problems for material design.

Due to the heavier computational burden of solving 3D topology optimization problems, our algorithm will be extended to 3D in future work based on some acceleration algorithms [30–32]. In addition, the extension of multi-material topology optimization based on the proposed TOP-IGA-MMC method will also be considered in the future.

### Supplementary

For the TOP-IGA-SIMP method, the problem of material design can be solved using the optimality criteria (OC) [25]. The density iteration formula is

$$p_e^{new} = \begin{cases} \max(0, \rho_e - m), & \text{if } \rho_e B_e^\eta \leq \max(0, \rho_e - m) \\ \min(0, \rho_e + m), & \text{if } \rho_e B_e^\eta \leq \min(0, \rho_e + m) \\ \rho_e B_e^\eta, & \text{otherwise} \end{cases} \quad (20)$$

where  $m$  ( $= 0.1$ ) is the step limit,  $\eta$  ( $= 1$ ) is the damping coefficient, and  $B_e^\eta$  is obtained by

$$B_e^\eta = - \left( \frac{\frac{\partial J}{\partial \rho_e}}{\lambda \frac{\partial V}{\partial \rho_e}} \right)^\eta. \quad (21)$$

where the Lagrange multiplier  $\lambda$  can be obtained by dichotomy. The sensitivity calculations are shown below:

$$\frac{\partial J}{\partial \rho_e} = \sum_{i=1}^3 \sum_{j=1}^3 \frac{\partial J}{\partial D_{ij}^H} \frac{1}{|V|} p \rho_e^{p-1} (E_0 - E_{min}) \left( d_e^{(i)} \right)^T \mathbf{K}_e d_e^{(j)}. \quad (22)$$

where  $\mathbf{K}_e^0$  is the stiffness matrix of the NURBS element with Young's modulus  $E_0$ . For more details on the OC criteria approach, see the literature [25, 33].

### Acknowledgements

This work is supported by the Provincial Natural Science Foundation of Anhui (2208085QA01), the Fundamental Research Funds for the Central Universities (WK0010000075), the National Natural Science Foundation of China (No. 61972368), and Research Grants Council (C4074-22GF), Innovation and Technology Commission (MRP/030/21, under PiH/273/22), Hong Kong Special Administrative Region, China.

### References

- [1] R. Jafari Nedoushan, Y. An, W.-R. Yu, New auxetic materials with stretch-dominant architecture using simple trusses, *Mechanics of Advanced Materials and Structures* (2021) 1-17.
- [2] D. R. Smith, N. Kroll, Negative refractive index in left-handed materials, *Physical Review Letters* 85 (14) (2000) 2933. <https://doi.org/10.1103/PhysRevLett.85.2933>
- [3] T. Ergin, N. Stenger, P. Brenner, J. B. Pendry, M. Wegener, Three-dimensional invisibility cloak at optical wavelengths, *Science* 328 (5976) (2010) 337-339. <https://doi.org/10.1126/science.1186351>
- [4] M. P. Bendsøe, N. Kikuchi, Generating optimal topologies in structural design using a homogenization method, *Computer Methods in Applied Mechanics and Engineering* 71 (2) (1988) 197-224. [https://doi.org/10.1016/0045-7825\(88\)90086-2](https://doi.org/10.1016/0045-7825(88)90086-2)
- [5] M. P. Bendsøe, Optimal shape design as a material distribution problem, *Structural Optimization* 1 (1989) 193-202. <https://doi.org/10.1007/BF01650949>
- [6] X. Huang, M. Xie, *Evolutionary topology optimization of continuum structures: methods and applications*, John Wiley & Sons, 2010. <https://doi.org/10.1002/9780470689486>
- [7] S. Osher, J. A. Sethian, Fronts propagating with curvature-dependent speed: Algorithms based on hamilton-jacobi formulations, *Journal of Computational Physics* 79 (1) (1988) 12-49. [https://doi.org/10.1016/0021-9991\(88\)90002-2](https://doi.org/10.1016/0021-9991(88)90002-2)
- [8] X. Guo, W. Zhang, W. Zhong, Doing topology optimization explicitly and geometrically a new moving morphable components based framework, *Journal of Applied Mechanics* 81 (8) (2014). <https://doi.org/10.1115/1.4027609>

- [9] W. Zhang, J. Yuan, J. Zhang, X. Guo, A new topology optimization approach based on moving morphable components (mmc) and the ersatz material model, *Structural and Multidisciplinary Optimization* 53 (2016) 1243-1260. <https://doi.org/10.1007/s00158-015-1372-3>
- [10] W. Zhang, W. Yang, J. Zhou, D. Li, X. Guo, Structural topology optimization through explicit boundary evolution, *Journal of Applied Mechanics* 84 (1) (2017). <https://doi.org/10.1115/1.4034972>
- [11] W. Zhang, L. Zhao, T. Gao, S. Cai, Topology optimization with closed b-splines and boolean operations, *Computer Methods in Applied Mechanics and Engineering* 315 (2017) 652-670. <https://doi.org/10.1016/j.cma.2016.11.015>
- [12] W. Zhang, Y. Liu, P. Wei, Y. Zhu, X. Guo, Explicit control of structural complexity in topology optimization, *Computer Methods in Applied Mechanics and Engineering* 324 (2017) 149-169. <https://doi.org/10.1016/j.cma.2017.05.026>
- [13] S. Zhang, A. L. Gain, J. A. Norato, A geometry projection method for the topology optimization of curved plate structures with placement bounds, *International Journal for Numerical Methods in Engineering* 114 (2) (2018) 128-146. <https://doi.org/10.1002/nme.5737>
- [14] W. Zhang, D. Li, J. Zhou, Z. Du, B. Li, X. Guo, A moving morphable void (mmv)-based explicit approach for topology optimization considering stress constraints, *Computer Methods in Applied Mechanics and Engineering* 334 (2018) 381-413. <https://doi.org/10.1016/j.cma.2018.01.050>
- [15] T. J. Hughes, *The finite element method: linear static and dynamic finite element analysis*, Courier Corporation, 2012.
- [16] J. Gao, M. Xiao, Y. Zhang, L. Gao, A comprehensive review of isogeometric topology optimization: methods, applications and prospects, *Chinese Journal of Mechanical Engineering* 33 (1) (2020) 1-14. <https://doi.org/10.1186/s10033-020-00503-w>
- [17] T. J. Hughes, J. A. Cottrell, Y. Bazilevs, Isogeometric analysis: Cad, finite elements, nurbs, exact geometry and mesh refinement, *Computer Methods in Applied Mechanics and Engineering* 194 (39-41) (2005) 4135-4195. <https://doi.org/10.1016/j.cma.2004.10.008>
- [18] J. Gao, L. Gao, Z. Luo, P. Li, Isogeometric topology optimization for continuum structures using density distribution function, *International Journal for Numerical Methods in Engineering* 119 (10) (2019) 991-1017. <https://doi.org/10.1002/nme.6081>
- [19] W. Hou, Y. Gai, X. Zhu, X. Wang, C. Zhao, L. Xu, K. Jiang, P. Hu, Explicit isogeometric topology optimization using moving morphable components, *Computer Methods in Applied Mechanics and Engineering* 326 (2017) 694-712. <https://doi.org/10.1016/j.cma.2017.08.021>
- [20] Y.-D. Seo, H.-J. Kim, S.-K. Youn, Isogeometric topology optimization using trimmed spline surfaces, *Computer Methods in Applied Mechanics and Engineering* 199 (49-52) (2010) 3270-3296. <https://doi.org/10.1016/j.cma.2010.06.033>
- [21] J. A. Cottrell, A. Reali, Y. Bazilevs, T. J. Hughes, Isogeometric analysis of structural vibrations, *Computer Methods in Applied Mechanics and Engineering* 195 (41-43) (2006) 5257-5296. <https://doi.org/10.1016/j.cma.2005.09.027>
- [22] P. Kang, S.-K. Youn, Isogeometric topology optimization of shell structures using trimmed nurbs surfaces, *Finite Elements in Analysis and Design* 120 (2016) 18-40. <https://doi.org/10.1016/j.finel.2016.06.003>

- [23] J. Gao, L. Wang, M. Xiao, L. Gao, P. Li, An isogeometric approach to topological optimization design of auxetic composites with tri-material micro-architectures, *Composite Structures* 271 (2021) 114163. <https://doi.org/10.1016/j.compstruct.2021.114163>
- [24] P. Theocaris, G. Stavroulakis, P. Panagiotopoulos, Negative poisson's ratios in composites with star-shaped inclusions: a numerical homogenization approach, *Archive of Applied Mechanics* 67 (1997) 274-286. <https://doi.org/10.1007/s004190050117>
- [25] B. Hassani, E. Hinton, A review of homogenization and topology optimization ihomogenization theory for media with periodic structure, *Computers & Structures* 69 (6) (1998) 707-717. [https://doi.org/10.1016/S0045-7949\(98\)00131-X](https://doi.org/10.1016/S0045-7949(98)00131-X)
- [26] W. Böhmer, Generating the b'ezier points of b-spline curves and surfaces, *Computer-Aided Design* 13 (6) (1981) 365-366. [https://doi.org/10.1016/0010-4485\(81\)90213-X](https://doi.org/10.1016/0010-4485(81)90213-X)
- [27] L. Xia, P. Breitkopf, Design of materials using topology optimization and energy-based homogenization approach in matlab, *Structural and Multidisciplinary Optimization* 52 (6) (2015) 1229-1241. <https://doi.org/10.1007/s00158-015-1294-0>
- [28] K. Svanberg, The method of moving asymptotes a new method for structural optimization, *International Journal for Numerical Methods in Engineering* 24 (2) (1987) 359-373. <https://doi.org/10.1002/nme.1620240207>
- [29] E. Andreassen, C. S. Andreasen, How to determine composite material properties using numerical homogenization, *Computational Materials Science* 83 (2014) 488-495. <https://doi.org/10.1016/j.commatsci.2013.09.006>
- [30] J. Martínez-Frutos, D. Herrero-Pérez, Large-scale robust topology optimization using multi-gpu systems, *Computer Methods in Applied Mechanics and Engineering* 311 (2016) 393-414. <https://doi.org/10.1016/j.cma.2016.08.016>
- [31] V. J. Challis, A. P. Roberts, J. F. Grotowski, High resolution topology optimization using graphics processing units (gpus), *Structural and Multidisciplinary Optimization* 49 (2) (2014) 315-325. <https://doi.org/10.1007/s00158-013-0980-z>
- [32] D. Zhang, X. Zhai, X.-M. Fu, H. Wang, L. Liu, Large-Scale Worst-Case Topology Optimization, *Computer Graphics Forum* (2022). doi:10.1111/cgf.14698. <https://doi.org/10.1111/cgf.14698>
- [33] S. S. Rao, *Engineering optimization: theory and practice*, John Wiley & Sons, 2019. <https://doi.org/10.1002/9781119454816>